Kinetics of lead and copper removal from oil-field brine by potential sorption

E. Nourafkan, M. Asachi and R. Marandi

ABSTRACT

The present study investigates the kinetics of lead and copper removal from oil-field brine by potential sorption. A population balance equation, coupled with a mass balance equation, was used in the estimation of kinetic parameters. Metal removal was performed by potential sorption of lead and copper through $CaCO_3$ precipitates induced by the reaction of Na_2CO_3 and $CaCl_2$. The oil-field brine was selected from an oil well in Gachsaran, Iran. The crystal size distribution of the solid phase was measured by dynamic laser scattering analyzer, and the liquor phase was analyzed using atomic adsorption. The morphology of calcium carbonate particles was illustrated using scanning electron microscopy and X-ray diffraction. The results showed that the presence of copper and lead decreases the average size distribution of calcium carbonate particles by influencing the kinetic parameters. Lead and copper concentrations were reduced from 2.911 to 0.127 ppm (95.63% removal) and 0.476 to 0.025 ppm (94.74% removal), respectively, in exchange for 12 g $CaCO_3$ consumption per 100 ml oil-field brine.

Key words | heavy metal, mass balance equation, population balance equation, potential sorption

E. Nourafkan (corresponding author)
Department of Chemical Engineering,
School of Chemical and Petroleum Engineering,
Shiraz University,
Shiraz 7134851154,
Iran
E-mail: *enorafkan@yahoo.com*

M. Asachi
R. Marandi
Department of Chemical Engineering,
North Tehran Branch, Islamic Azad University,
Tehran,
Iran

NOMENCLATURE

a	Growth rate order with respect to supersaturation, dimensionless
$B(v,t)$	Birth function (#/s/μm^3)
B°	Nucleation rate (#/s)
C	Agglomeration kernel (1/#/s)
$[Ca^{2+}]$	Concentration of calcium ion (mol/l)
$[CO_3^-]$	Concentration of carbonate ion (mol/l)
$D(v,t)$	Death function (#/s/μm^3)
G_L	Growth rate of adduct particles (μm/s)
G_v	Growth rate of adduct particles (μm^3/s)
k_c	Agglomeration rate coefficient (1/#/s/μm^3)
k_g	Coefficient of growth rate equation (μm/s)
k_n	Coefficient of nucleation rate equation (#/s)
k_{sp}	Solubility product constant ((mol/l)^3)
k_v	Shape factor, dimensionless
M_T	Magma density of crystals ($g_{crystal}$)
n	Crystal population density (#/μm^3)
N_e	Number of experiments, dimensionless
N_M	Number of dynamic laser scattering analysis data point, dimensionless
N_S	Number of measures supersaturation by atomic adsorption, dimensionless
S	Supersaturation, dimensionless
t	Time (s)
Q	Mass flow rate of net calcium chloride (g $CaCl_2$/s)
Mw_{CaCl_2}	Molecular weight of calcium chloride (kg/kmol)
Mw_{CaCo_3}	Molecular weight of calcium carbonate (kg/kmol)
V	Volume of solution (l)
u	Crystal volume (μm^3)
v	Crystal volume (μm^3)
Φ	Objective function, dimensionless

INTRODUCTION

Industrial effluents containing large amounts of dissolved heavy metals are of increasing concern due to their toxicity and non-biodegradability (Jamil *et al.* 2010). Heavy metal contamination exists in the aqueous waste stream from many industries such as desalination of oil, metal plating,

doi: 10.2166/wst.2014.444

mining and painting (Sdiri *et al.* 2012). Oil-field brine containing heavy metals (Pb, Cu, Ni and Cr) is separated from oil by well-head operation and is usually returned to the reservoir for water flooding or is discarded to the surroundings (Habibnia & Dinarvand 1998; Igunnu & Chen 2012; Namdari *et al.* 2012). Therefore, the water and soil around the well may be polluted due to probable contact with discarded water.

Cu(II) and Pb(II) ions are among the most common heavy metals in oil-field effluents. The accumulation of these contaminants in the human body can cause severe health risks.

Potential sorption processes are widely used to remove metal ions from solution. Potential sorption mechanisms include inner or outer-sphere adsorption, co-precipitation (whereby the metal ion is incorporated into the particle structure to form a dilute solid-solution) and precipitation of discrete metal phases. Owing to the ubiquity, reactivity and low price of calcium carbonate, this mineral presents a viable substrate for effective heavy-metal removal using potential sorption mechanisms (Rouff *et al.* 2002; Khosravi & Alamdari 2009). Furthermore, an abundance of calcium ion in oil-field brine suggests that precipitation of calcium carbonate for metal removal would perhaps be economically promising. Hong *et al.* (2011) have investigated the use of carbonate precipitation to treat effluents containing heavy metals. In addition, Ahmad *et al.* (2012) studied the adsorption of heavy metal ions in a continuous flow column with calcium carbonate as adsorbent. The aqueous solution of heavy metals is passed through the column, forming a bed of precipitated $CaCO_3$. According to their results, it was concluded that calcium carbonate may act as an efficient adsorbing material for the adsorption of heavy metal ions from aqueous solution. The calcium carbonate may reduce the level of heavy metals by more than 99%.

Khosravi & Alamdari (2009) investigated the interaction of calcium carbonate with copper in aqueous solutions. They reported 78% removal of copper by reducing Cu^{2+} concentration from 0.27 to 0.06 ppm. They used 1 g of precipitate per 0.15 mg copper metal for removal. In addition, the analysis of their experiment suggested that about 5% of the copper removal from the synthetic brine occurred through the mechanism of incorporation into the crystal lattice, and around 95% occurred through adsorption on the crystal faces.

The Pb^{2+} ions can be removed from solution through absorbance by two coordination bonds at the surface of the calcium carbonate particles. In addition to adsorption, the co-precipitation mechanism was completed by the entrance of lead ions in the crystal structure of calcium carbonate through the formation of six-fold coordination bonds. Co-precipitation and adsorption of lead by calcium carbonate particles was investigated by Fulghum *et al.* (1988). Pb^{2+} ions can be precipitated as $PbCO_3$ species on the crystal surface. These complexes are likely to be the form in which Pb^{2+} interacts at kink sites. Thus, the introduction of Pb^{2+} and subsequent sorption of $PbCO_3$ complexes at kink sites may inhibit step-kink motion, ultimately reducing microscopic precipitation and dissolution (Rouff *et al.* 2005).

In this study, the effects of copper and lead on $CaCO_3$ precipitation was investigated by a solution population balance equation and mass balance equation simultaneously.

EXPERIMENTAL

The experiment components, including calcium chloride, sodium carbonate, calcium carbonate, lead nitrate and copper nitrate were provided from Merck Company (Munich, Germany). The experiments were carried out semi-batch wise in a 1-l reactor schematically shown in Figure 1. The optimum value of 24 °C for temperature, 13 for pH and 30 minutes for the addition time of reactant were specified in a previous study of Asachi & Marandi (2014) on the design of experimental method.

The precipitation reaction was performed in three different solutions as follows:

1. Pure solution containing deionized water (50 ml) and sodium carbonate (50 ml, 2.5 M).
2. Synthetic solution containing deionized water (50 ml), sodium carbonate (50 ml, 2.5 M), lead nitrate (20 ml, 9.78 ppm) and copper nitrate (20 ml, 9.1 ppm).
3. Oil-field brine from Gachsaran in Iran (100 ml) (the analysis of oil-field brine is shown in Table 1).

To prevent homogenous nucleation, the calcium chloride solution (25 ml, 5 M) was added to the reactor by an infusion pump (OT-701 type, JMS Co., California, USA) over 30 minutes. Furthermore, to prevent excessive nucleation, 0.5 g of calcium carbonate was added as seed before the commencement of the reaction, and the mixer speed was set to 200 rpm. Each semi-batch experiment was performed three times for the statistical analysis of optimum kinetic parameters.

Some important properties of calcium carbonate crystal are shown in Table 2.

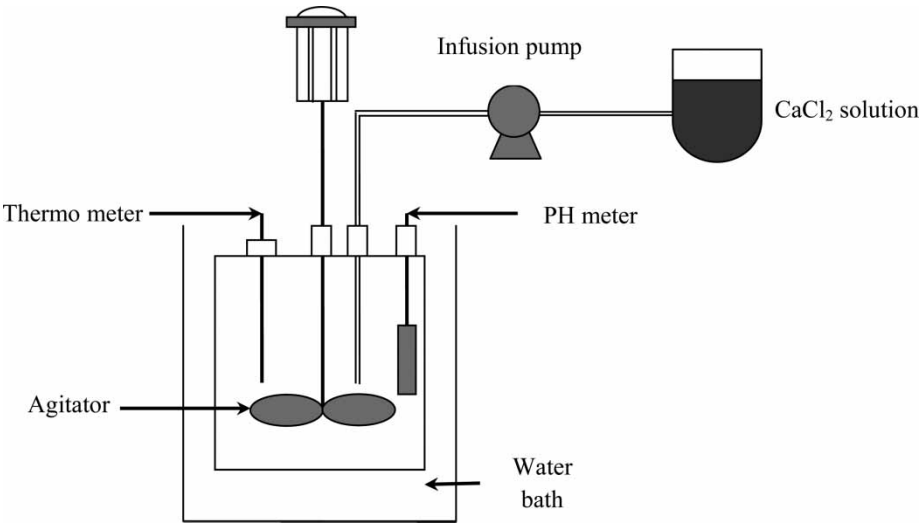

Figure 1 | A schematic diagram of the experimental setup.

Table 1 | The composition of a brine sample from Gachsaran oil field in Iran

Parameter	Value
pH	5.7
Total dissolved solids (g/l)	174
Turbidity (NTU)	2.7
Conductivity (μs/cm)	705
Ca^{2+} (mg/l)	1,799
Na^{+} (mg/l)	22,154
Cl^{-} (mg/l)	44,772
Mg^{2+} (mg/l)	7,806
SO_4^{2-} (mg/l)	567
Cu^{2+} (ppm)	0.476
Pb^{2+} (ppm)	2.911

Table 2 | Some important properties of calcium carbonate crystal

Properties of $CaCO_3$ crystals	Molecular weight (g/mol)	Shape factor	Density (g/cm^3)	k_{sp}
Value	100.086	32[a]	2.71	4.8×10^{-9}

[a]Ahn *et al.* (2005).

The size distribution of particles was measured by a dynamic laser scattering analyzer (Malvern Master Sizer 2000 Malvern company, Worcestershire, UK). The concentration of lead and copper in the solution was measured by atomic adsorption (Varian AA 240, Varian Inc., California, USA). The morphology of resulting particles was characterized by a high resolution scanning electron microscope (Hitachi S-4160, Hitachi Co., Tokyo, Japan) operating at 20 kV. The sample was prepared by coating it with a very thin gold layer, which was deposited by sputtering under vacuum.

At the end of the experiments, the suspension in the crystallizer was filtered and dried in an oven at 80 °C to be prepared for X-ray diffraction (XRD) analysis. XRD analysis was performed by StoeStadi P working with Cu Kα radiation, $\lambda = 1.540$, Å40 kV and 40 mA. The XRD pattern was analyzed by X'Pert HighScore software (Plus v3.0), and the different phases were determined by comparing XRD peaks with the ASTM standard.

MATHEMATICAL MODELING

Equations of mass and population balances were coupled with appropriate initial and boundary conditions in order to model the precipitation of $CaCO_3$. The population balance equation for a batch or semi-batch precipitation process in the absence of particle breakage is as follows:

$$\frac{\partial n(v,t)}{\partial t} + \frac{\partial (G_v n(v,t))}{\partial v} = B(v,t) - D(v,t) \quad (1)$$

The growth, nucleation, birth and death function are given by the following equations (Randolph & Larson 1988):

$$B^{o} = k_n M_T S \quad (2)$$

$$G_L = k_g S^a \quad (3)$$

$$B(t,v) = \frac{1}{2}\int_0^v C(u, v-u)\, n(v-u, t)\, n(u, t)\, du \tag{4}$$

$$D(t,v) = n_v(v, t)\int_0^\infty C(v, u)\, n(u, t)\, du \tag{5}$$

where C is the agglomeration kernel, u and v are the particle volumes. Some similarities between mixing pattern in the draft tube, the annulus space of the crystallizer of the present study and that of the shear stream, and strong dependence of agglomeration to supersaturation led to the following kernel function:

$$C(v,u) = k_c\left(u^{\frac{1}{3}} + v^{\frac{1}{3}}\right)^3 \tag{6}$$

The growth rate based upon particle volume is

$$G_v = 3k_g k_v^{1/3} S^a v^{2/3} \tag{7}$$

The dimensionless supersaturation is calculated as follows (Skoog *et al.* 2013):

$$S = \frac{[Ca^{2+}][CO_3^{2-}] - k_{sp}}{k_{sp}} \tag{8}$$

The concentrations of calcium and carbonate ion are calculated by mass balance equation as follows:

$$\frac{d(V[Ca^{2+}])}{dt} = \frac{Q}{Mw_{CaCl_2}} - \frac{1}{Mw_{CaCO_3}}\frac{dM_T}{dt} \tag{9}$$

$$\frac{d(V[CO_3^{2-}])}{dt} + \frac{1}{Mw_{CaCO_3}}\frac{dM_T}{dt} = 0 \tag{10}$$

The reaction between $CaCl_2$ and $CaCO_3$ generates solute mass in the solution and the particle growth consumes mass from the solution and deposits it on the solid phase. Equation (9) calculates the changes in Ca^{2+} concentrations by the relation between mass deposition on $CaCO_3$ particles and the entrance mass of $CaCl_2$ reagent in solution, and Equation (10) calculates the carbonate concentrations by the relation between mass deposition on $CaCO_3$ particles and total rest mass of carbonate in solution. The boundary conditions for solving the mass equations are as follows:

$$Ca^{2+}(t=0) = 0, \quad CO_3^{2-}(t=0) = CO_{3,ini}^{2-} \tag{11}$$

The kinetic parameters in the rate equations are adjusted to minimize the deviations between the model predictions of particle size distribution (PSD) and those measured experimentally. Therefore, the optimal sets of parameters were found by solving the nonlinear optimization problem as follows:

$$\min \Phi(k_g, k_n, a, k_c)$$
$$\Phi(\theta) = \sum_{j=1}^{N_M}\left(\frac{n_{exp}(j) - n_{mod}(j)}{n_{exp}(j)}\right)^2 \times \sum_{k=1}^{N_s}\left(\frac{S_{exp}(k) - S_{mod}(k)}{S_{exp}(k)}\right)^2 \tag{12}$$

Ramachandran & Barton (2010) consider the solution of optimization problems with a multi-dimensional population balance model using the Nelder–Mead simplex method (fminsearch routine), Broyden–Fletcher–Goldfarb–Shanno (BFGS) quasi-Newton (Fminunc routine), Gauss–Newton (Lsqnonlin routine) and sequential quadratic programming (SQP) (fmincon routine).

In this research, 'fmincon routine' was used for minimization of the objective function and the best values of kinetic parameters were estimated. Fmincon uses an SQP method. In this method, the function solves a quadratic program at each iteration. Fmincon updates an estimate of the Hessian of the Lagrangian at each iteration using the BFGS formula (Fletcher & Powell 1963; Goldfarb 1970).

NUMERICAL SOLUTION

Simultaneous solution of mass and population equations, using the numerical implicit method of Crank–Nicolson, calculated the population density of particles and size distributions of product at various times (Alamdari *et al.* 2010). The following finite difference equations were substituted in the main population balance equation:

$$n(t,v) = n_{i,j} \tag{13}$$

$$\frac{\partial n}{\partial t} = \frac{n_{i+1,j} - n_{i,j}}{\Delta t} \tag{14}$$

$$\frac{\partial n}{\partial v} = \frac{\partial n}{\partial \log v} \times \frac{\partial \log v}{\partial v} = \frac{\partial n}{\partial \log v} \times \frac{\log e}{v} \tag{15}$$

$$\frac{\partial n}{\partial \log v} = \frac{1}{2}\left[\frac{n_{i,j+1} - n_{i,j-1}}{2\Delta \log v} + \frac{n_{i+1,j+1} - n_{i+1,j-1}}{2\Delta \log v}\right] \tag{16}$$

For the incensement of tiny particle volumes that produced a greater number of particles, the logarithmic size increment was used (Alamdari *et al.* 2000). By mathematical arrangement, the following equation was obtained:

$$+\gamma_2 n_{i+1,j+1} + n_{i+1,j} - \gamma_2 n_{i+1,j-1} = -\gamma_2 n_{i,j+1} + (1-\gamma_1) n_{i,j} + \gamma_2 n_{i,j-1} \quad (17)$$

$$\gamma_1 = 2k_g k_v^{\frac{1}{3}} S^a v^{\frac{-1}{3}} \Delta t \quad (18)$$

$$\gamma_2 = \frac{3k_g k_v^{\frac{1}{3}} S^a v^{\frac{-1}{3}} \Delta t . \log e}{4\Delta \log v} \quad (19)$$

Using Matlab software, Equations (17) and (18) are converted to a matrix of coefficients and were solved for different times (Thomas 1995).

RESULTS AND DISCUSSION

SEM and XRD observation

The scanning electron microscopy (SEM) images of the precipitates from three different solutions (pure solution, synthetic solution and oil-field brine) are shown in Figure 2.

The morphology of precipitates from pure solution was the rhombohedral calcite crystal. Figure 2(b) shows the effect of copper and lead on the $CaCO_3$ morphology. According to Figure 2(b), the sorption of Pb^{2+} and Cu^{2+} ions on the $CaCO_3$ caused the surface change of the crystals. However, the morphology of crystals in synthetic solution is still calcite while the structure of crystals has more defects compared to the pure solution. In addition, these defects may appear due to the adsorption of the cerussite phase on the surface of $CaCO_3$ crystals, thus disrupting surface growth. Figure 2(c) shows the presence of globular vaterite crystals accompanied by rhombohedral calcite, which may be attributed to the presence of abundant impurities in the industrial brine.

The XRD pattern of calcium carbonate precipitate from synthetic solution and oil-field brine is shown in Figure 3.

The XRD pattern of synthesis solution (Figure 3(a)) shows the presence of calcite, cerussite ($PbCO_3$) and copper carbonate ($CuCO_3$). The appearance of cerussite suggested that one mechanism of lead removal was the precipitation of $PbCO_3$, probably on the $CaCO_3$ particles, in addition to surface adsorption and incorporation in the crystal lattice (Godelitsas *et al.* 2004; Chada *et al.* 2005).

XRD and SEM analysis of precipitates from the oil-field brine resulted in the existence of aragonite and vaterite morphology besides calcite, and this was due to extra impurities in the oil-field brine, such as nickel as seen in Figure 3(b).

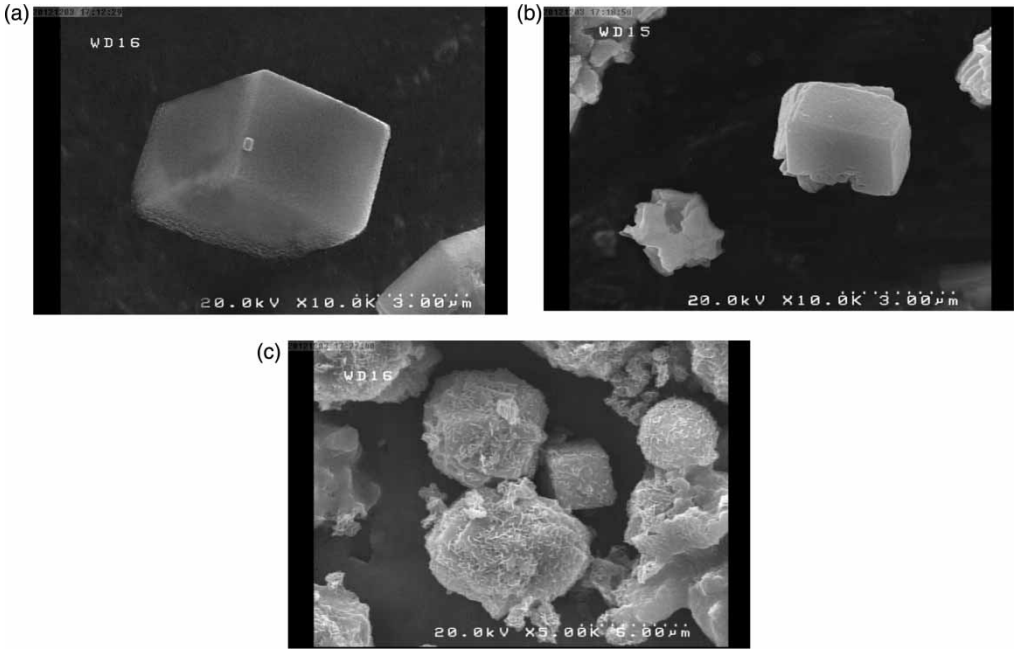

Figure 2 | SEM photomicrograph showing the calcium carbonate particles precipitated from (a) pure solution, (b) synthetic solution and (c) oil-field brine.

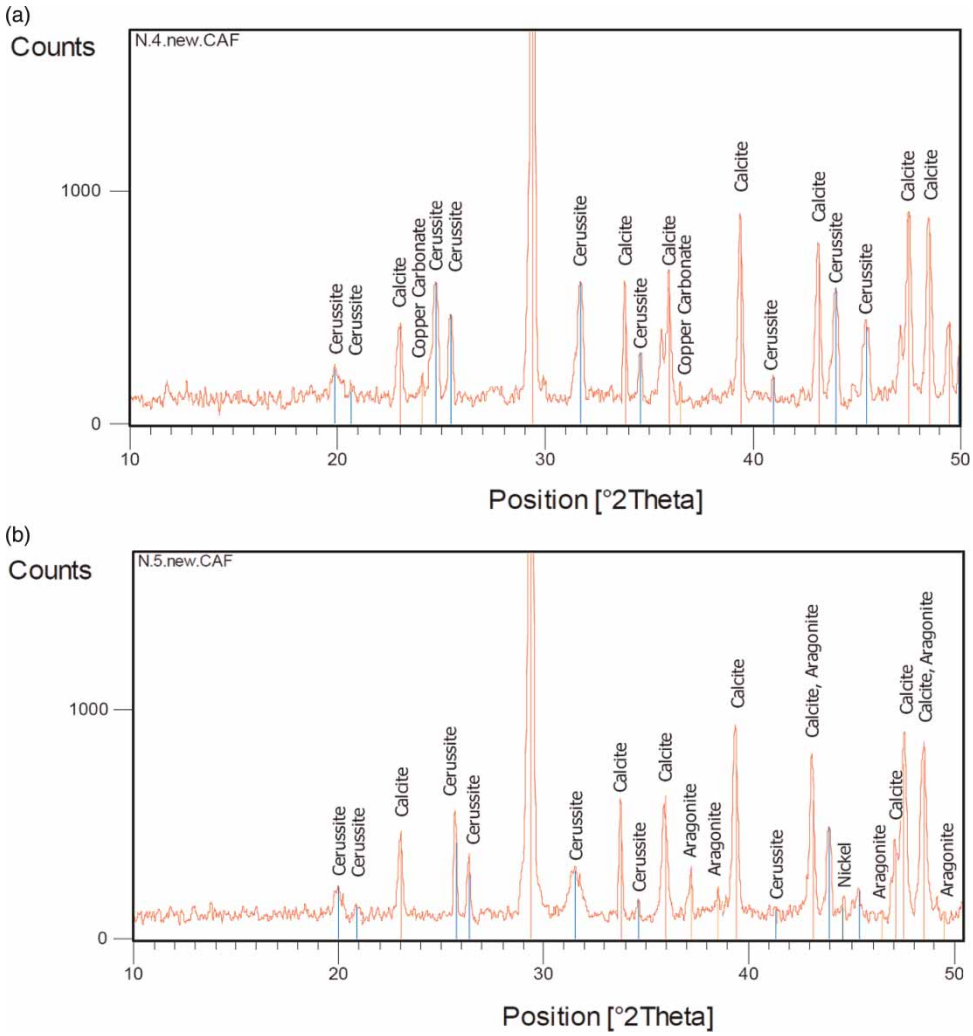

Figure 3 | The XRD pattern of calcium carbonate particles precipitated from (a) synthetic solution and (b) oil-field brine.

Optimum kinetic parameters

The final cumulative undersize distribution and supersaturation of three experiments after 30 minutes for pure solution are shown in Figures 4 and 5, respectively.

The consistency of experimental results suggests that the particle size distributions of products are almost reproducible. The optimization process was individually carried out using data from each run of experiments and mean value and standard error of obtained parameters were calculated. The mean values and the standard error of kinetic parameters of growth, nucleation and agglomeration rates, for precipitation from pure solution, synthetic solution and oil-field brine, are reported in Table 4. Mean value and standard error of parameters were calculated from the following equations:

$$\bar{x} = \frac{\sum_{i=1}^{n_e} x_i}{n_e} \tag{20}$$

$$\text{S.E.} = \frac{\sqrt{\sum_{i=1}^{n_e} (x_i - \bar{x})^2/(n_e - 1)}}{\sqrt{n_e}} \tag{21}$$

where x_i represents the optimum value of each parameter and n_e is the number of repetition of each experiment.

The final cumulative undersize distribution of precipitates from pure solution, synthetic solution and oil-field brine is shown in Figure 6.

According to Figure 6, the presence of heavy metal ions in solution leads to a decrease in the average size

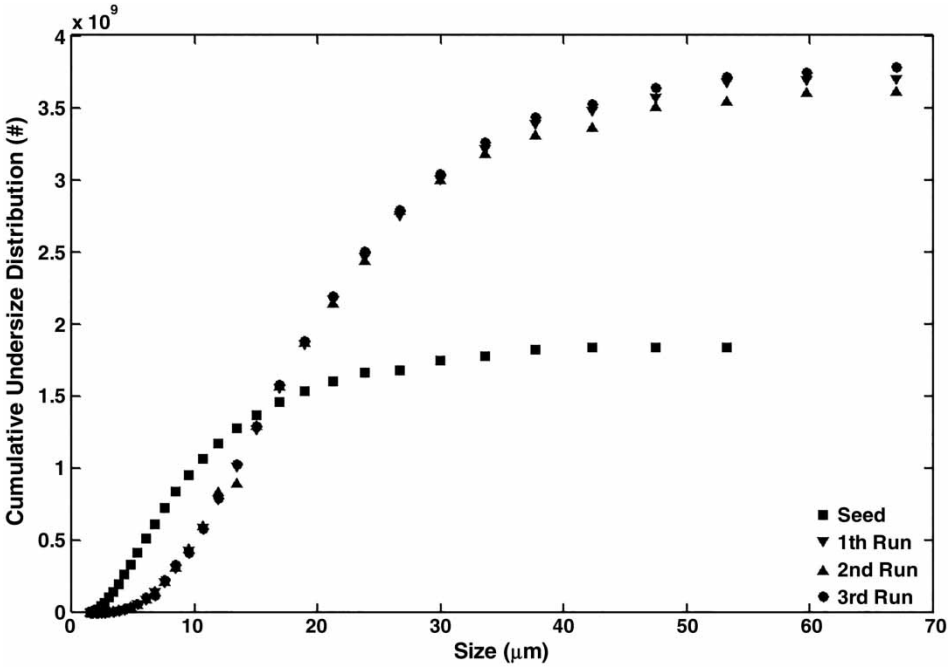

Figure 4 | The cumulative undersize distribution of precipitated $CaCO_3$ from pure solution (three runs).

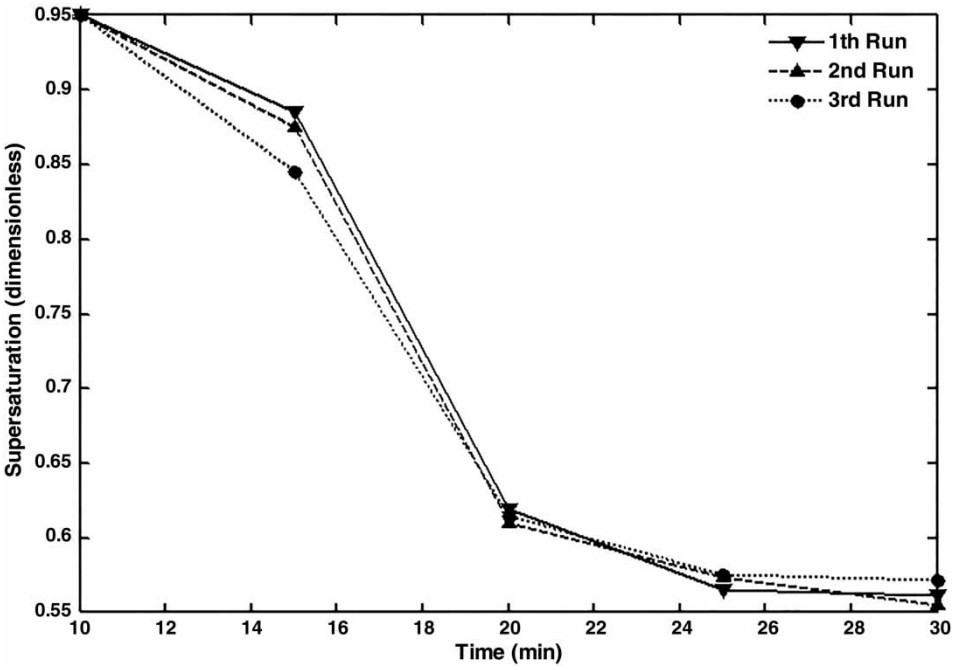

Figure 5 | The experimentally measured supersaturation for pure solution (three runs).

of crystals. Therefore, it seems that heavy metal ions either sorbed on the surface of the crystal or substituted the interior crystal structure of calcium ions, leading to kinetics changes. Some specifications of the final precipitation from different solutions are shown in Table 3.

The experimental crystal size distribution data obtained from precipitation experiments were used to optimize the

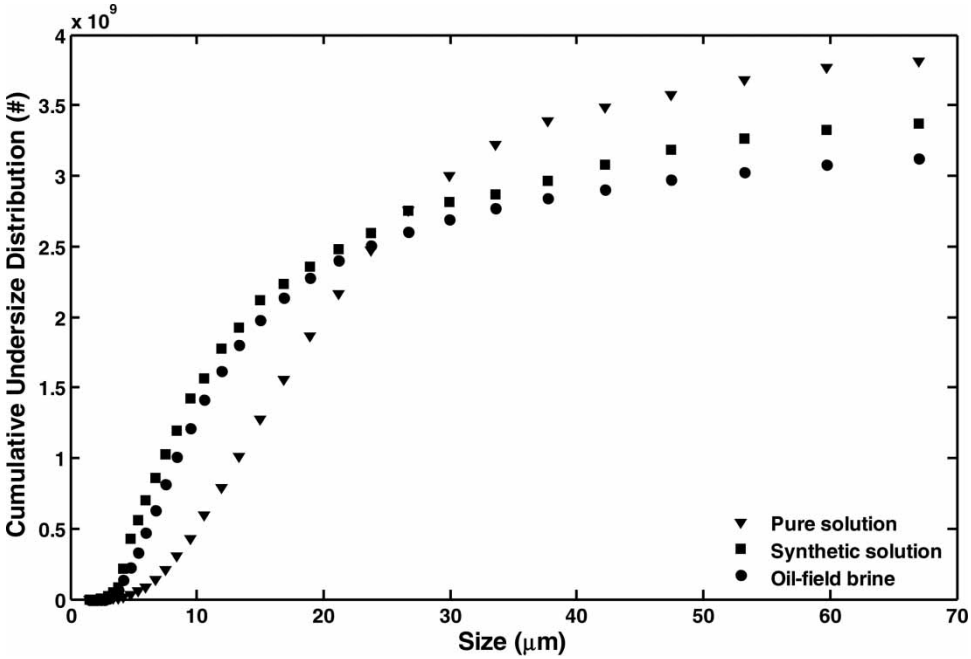

Figure 6 | The cumulative undersize distribution of precipitated $CaCO_3$ from pure solution, synthetic solution and oil-field brine.

Table 3 | Some properties of final precipitates

Solutions	Pure	Synthetic	Oil-field brine
Volume weighted mean diameter, $D_{4,3}$ (μm)	22.19	19.36	15.00
Mass of product (g)	14.4	13.15	12.39
$d_{0.5}$ (μ)	19.92	12.93	9.94
Initial lead concentration (ppm)	–	9.78	2.911
Final lead concentration (ppm)	–	0.061	0.127
Initial copper concentration (ppm)	–	9.1	0.476
Final copper concentration (ppm)	–	0.097	0.025

Table 4 | Optimum values of kinetic parameters of calcium carbonate precipitation from pure solution, synthetic solution and oil-field brine

Parameter	Pure solution	Synthetic solution	Oil-field brine
k_g (μm/s)			
Mean value	7.53×10^{-9}	3.14×10^{-9}	1.05×10^{-9}
Standard error	0.202×10^{-9}	0.073×10^{-9}	0.112×10^{-9}
k_n (#/s)			
Mean value	9.68×10^{-8}	8.01×10^{-8}	4.33×10^{-8}
Standard error	0.095×10^{-8}	0.255×10^{-8}	0.301×10^{-8}
k_c (1/#/s/μm^3)			
Mean value	2.33×10^{-17}	3.61×10^{-17}	8.07×10^{-17}
Standard error	0.067×10^{-17}	0.078×10^{-17}	0.112×10^{-17}
a (–)	1.51	1.81	1.91
MAPD[a]	4.43	5.17	6.36

a: mean absolute percentage deviation $= \frac{1}{n}\sum_{i=1}^{n}\left|\frac{(n_{\mathrm{mod}}(i)-n_{\exp}(i))}{n_{\exp}(i)}\right|\times 100.$

kinetic parameters. Figure 7 shows a comparison of experimental data with model predictions of crystal size distribution. The optimum values of kinetic parameters are reported in Table 4. Furthermore, the values of mean absolute percentage deviation (MAPD) of fitting data are presented in Table 4. MAPD is a criterion of the accuracy of fitted values compared with experimental data. The MAPD values near 5% in Table 4 show a good fitting of model to experimental data.

According to kinetic parameters of pure and synthesis solution, heavy metal ions cannot disrupt the nucleation and growth mechanism significantly. So this metal trace did not block the active sites of the $CaCO_3$ crystals. In fact, copper and lead ions were substituted instead of calcium ions in the crystal lattice of $CaCO_3$. But a decrease in crystal size (Table 3) is probably due to adsorption of the cerussite phase on the surface of crystals. In addition, the new bond of copper and lead ions in the $CaCO_3$ lattice can change the growth mechanism of crystals and decrease the average size.

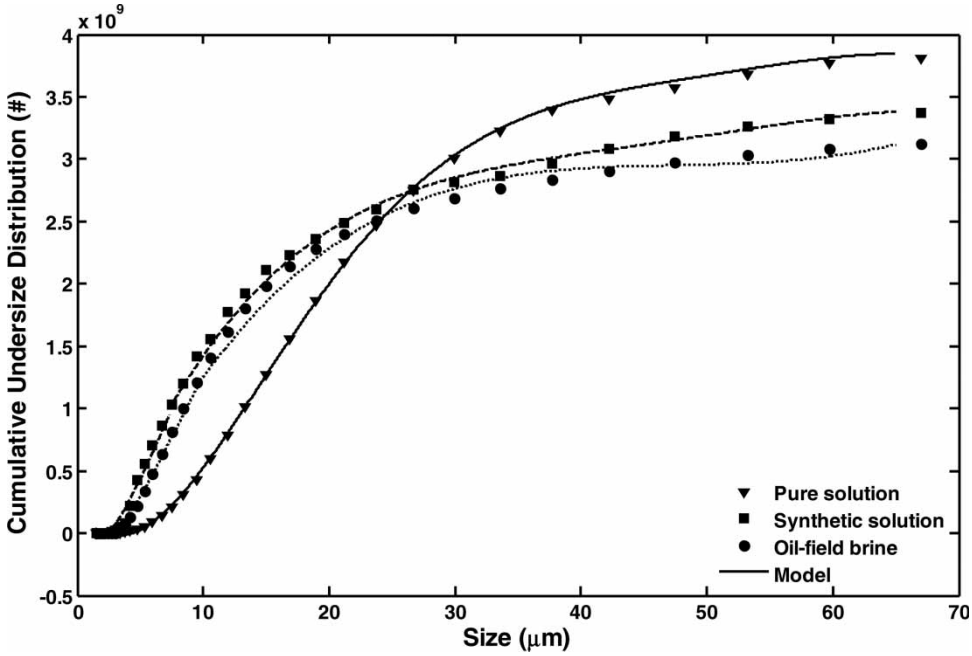

Figure 7 | Comparison of experimental cumulative undersize distribution and model predictions.

Figure 8 shows that the model predicted supersaturation and those calculated from experimental data during the addition of $CaCl_2$. As shown in Figure 8, in the pure solution, the supersaturation is higher than in the synthesis solution and oil-field brine. This indicates that heavy metal traces inhibit supersaturation release on nucleation and growth mechanisms, and therefore, a decrease in productivity occurs for solution containing heavy metal traces (Figure 9). The maximum points in Figure 8 represent the time at which the amount of produced supersaturation

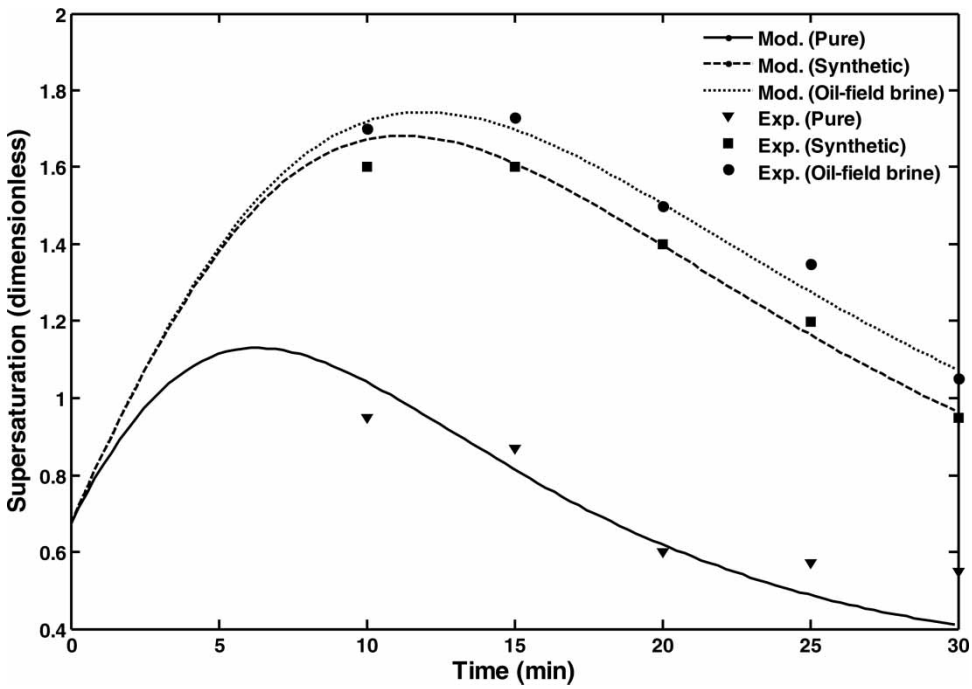

Figure 8 | The experimentally measured and the model predictions of supersaturation.

becomes equal to the amount of supersaturation consumption because of growth and nucleation.

The comparisons of the produced crystal total the mass predicted by the model, and experimental results are shown in Figure 9.

To verify the reliability of model parameters, and clarify the model sensitivity to rate parameters, the value of each parameter around its optimum point was varied, when other parameters were kept constant, and the changes in objective function were monitored. Sufficient variations in

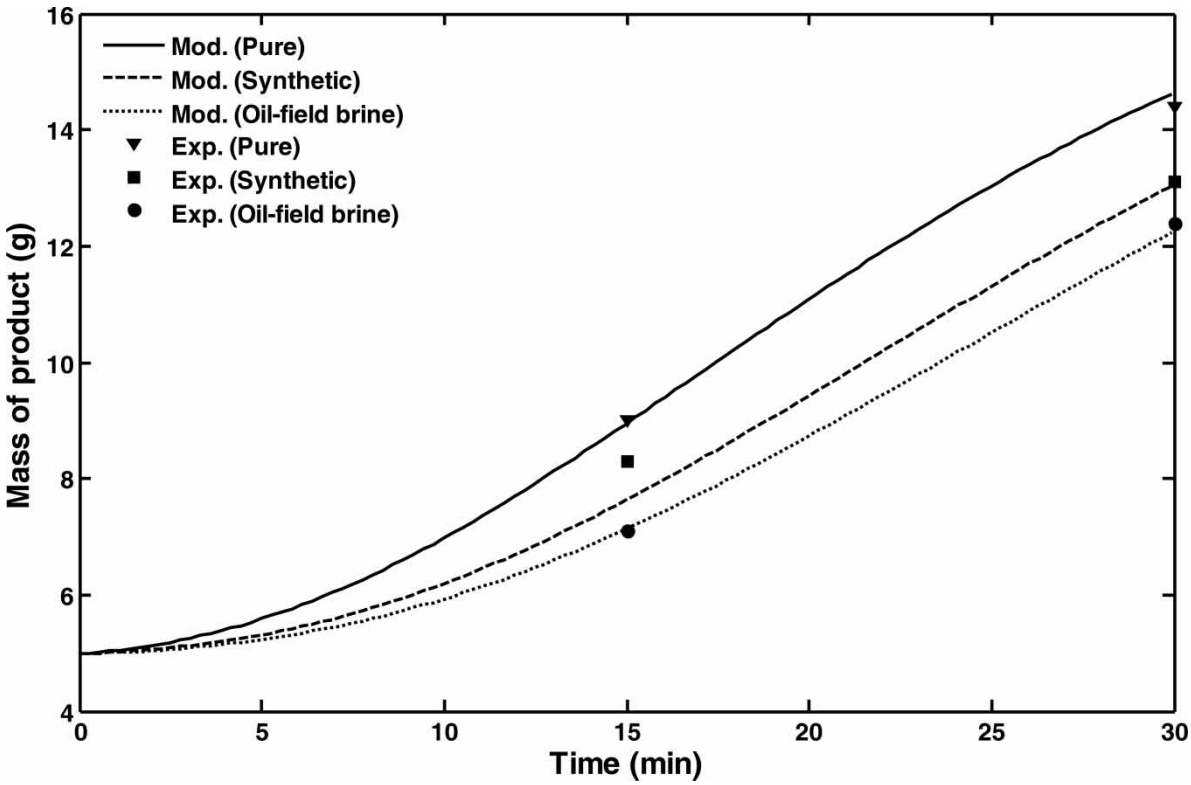

Figure 9 | Comparisons of total mass between experimental data and model predictions.

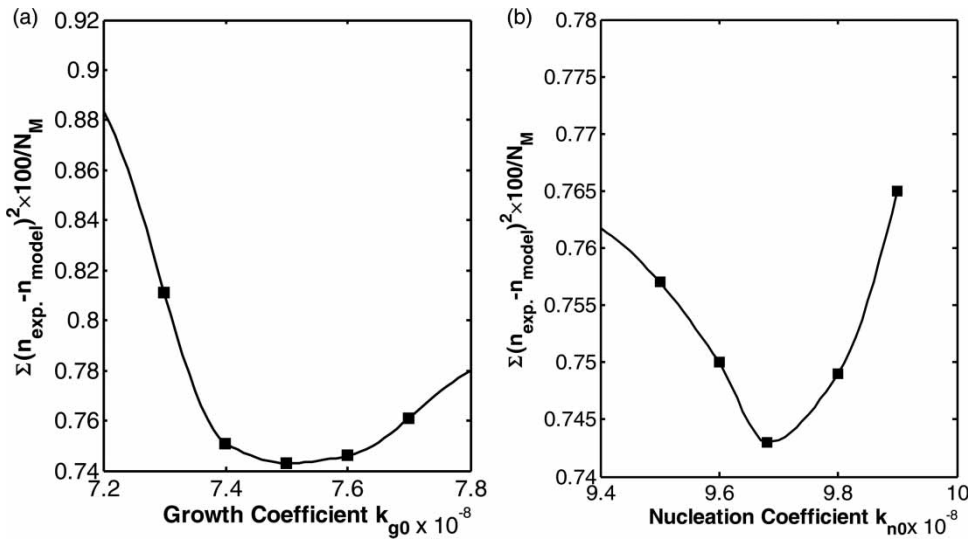

Figure 10 | Sensitivity analysis of objective function with (a) changes of growth coefficient and (b) changes of nucleation coefficient near the optimum point for the case of pure solution.

the values of objective function for parameters of growth, nucleation and agglomeration rates were suggestive of the reliability of these parameters. For brevity, the sensitivity of objective function with respect to nucleation and growth coefficients was only shown in Figure 10.

CONCLUSION

The mechanisms of nucleation, growth and agglomeration for calcium carbonate precipitation from pure solution, synthetic solution and oil-field brine were modeled, and the rate equation parameters were optimized. The presence of lead and copper ions in the liquor reduced the average size of crystals, nucleation and growth. The presence of Pb^{2+} and Cu^{2+} ions causes surface change of crystals due to the sorption of ions on the surface of $CaCO_3$ crystals. The impurities in the industrial brine led to the observation of globular vaterite crystals in company with rhombohedral calcite. Lead and copper concentrations were reduced from 2.911 to 0.127 ppm (95.63% removal) and 0.476 to 0.025 ppm (94.74% removal), respectively, in exchange for 12 g $CaCO_3$ consumption per 100 ml oil-field brine.

REFERENCES

Ahmad, K., Bhatti, I. A., Muneer, M., Iqbal, M. & Iqbal, Z. 2012 Removal of heavy metals (Zn, Cr, Pb, Cd, Cu and Fe) in aqueous media by calcium carbonate as an adsorbent. *International Journal of Chemical and Biochemical Sciences* **2**, 48–53.

Ahn, J. W., Kim, J. H., Park, H. S., Kim, J. A., Han, C. & Kim, H. Synthesis of single phase aragonite precipitated calcium carbonate in $Ca(OH)_2$-Na_2CO_3-NaOH reaction system. *Korean Journal of Chemical Engineering* **22** (2005), 852–856.

Alamdari, A., Raper, J. A. & Wainwright, M. S. 2000 A model for aluminium trihydroxide crystallization from pure and impure solutions. *Chemical Engineering Communications* **180**, 83–105.

Alamdari, A., Nourafkan, E. & Jahanmiri, A. 2010 Model development for deactivation of bisphenol-A adduct particles during crystallization under the influence of impurity. *Journal of Crystal Growth* **312**, 2247–2253.

Asachi, M. & Marandi, R. 2014 Response surface modeling of lead and copper removal from oil field brine by potential sorption method. *Particulate Science and Technology* (in press).

Chada, V. G. R., Hausner, D. B., Strongin, D. R., Rouff, A. A. & Reeder, R. J. 2005 Divalent Cd and Pb uptake on calcite {1014} cleavage faces: an XPS and AFM study. *Journal of Colloid and Interface Science* **288**, 350–360.

Fletcher, R. & Powell, M. J. D. 1963 A rapidly convergent descent method for minimization. *Computer Journal* **6**, 163–168.

Fulghum, J. E., Bryant, S. R. & Linton, R. W. 1988 Discrimination between adsorption and coprecipitation in aquatic particle standards by surface analysis techniques: lead distributions in calcium carbonates. *Environmental Science and Technology* **22**, 463–467.

Goldfarb, D. 1970 A family of variable metric updates derived by variational means. *Mathematics of Computing* **24**, 23–26.

Godelitsas, A., Astilleros, J. M., Hallam, K., Harissopoulos, S. & Putnis, A. 2004 Interaction of calcium carbonates with lead in aqueous solutions. *Environmental Science and Technology* **37**, 3351–3360.

Habibnia, B. & Dinarvand, A. 1998 The effect of discharging salty oil field effluents on southern environmental pollution of Iran. In: *3rd National Conference of Chemical Engineering*. Ahvaz University, Iran, pp. 730–736.

Hong, K. S., Lee, H. M., Bae, J. S., Ha, M. G., Jin, J. S., Hong, T. E., Kim, J. P. & Jeong, E. D. 2011 Removal of heavy metal ions by using calcium carbonate extracted from starfish treated by protease and amylase. *Journal of Analytical Science and Technology* **2**, 75–82.

Igunnu, E. T. & Chen, G. Z. 2012 Produced water treatment technologies. *International Journal of Low-Carbon Technologies* **1**, 1–21.

Jamil, M., Zia, M. S. & Qasim, M. 2010 Contamination of agro-ecosystem and human health hazards from wastewater used for irrigation. *Journal of Chemical Society of Pakistan* **32**, 370–378.

Khosravi, J. & Alamdari, A. 2009 Copper removal from oil-field brine by coprecipitation. *Hazardous Materials* **166**, 695–700.

Namdari, A., Mazarei, Z. & Tahernejad, T. 2012 A comprehensive plan presentation on the generating wastes management in Ahvaz oil production and desalinization plants, on the RCRA Basis. *Annals of Biological Research* **3**, 5379–5389.

Ramachandran, R. & Barton, P. 2010 Effective parameter estimation within a multi-dimensional population balance model framework. *Chemical Engineering Science* **65**, 4884–4893.

Randolph, A. D. & Larson, M. A. 1988 *Theory of Particulate Processes*, 2nd edn. Academic Press, New York.

Rouff, A. A., Reeder, R. J. & Fisher, N. S. 2002 Pb(II) sorption with calcite: a radio tracer study. *Aquatic Geochemistry* **8**, 203–228.

Rouff, A. A., Elzinga, E. J., Reeder, R. J. & Fisher, N. S. 2005 The influence of pH on the kinetics, reversibility and mechanisms of Pb(II) sorption at the calcite–water interface. *Geochimica et Cosmochimica Acta* **69**, 5173–5186.

Sdiri, T., Higashi, F. J. & Bouaziz, S. 2012 Effects of impurities on the removal of heavy metals by natural limestones in aqueous systems. *Journal of Environmental Management* **93**, 245–253.

Skoog, D. A., West, D. M., Holler, J. & Crouch, S. R. 2013 *Fundamentals of Analytical Chemistry*, 9th edn. Cengage Learning, Belmont, California, USA.

Thomas, J. W. 1995 *Numerical Partial Differential Equations: Finite Difference Methods*, 1st edn. Springer, Berlin, New York. Corr. 2nd printing 1998 edition.

First received 23 March 2014; accepted in revised form 27 October 2014. Available online 10 November 2014